



Article

2013–2014 Survey of Chars Using Raman Spectroscopy

John McDonald-Wharry

School of Engineering, The University of Waikato, Hamilton 3240, New Zealand;
john.mcdonald-wharry@waikato.ac.nz; Tel.: +64-07-838-4466 (ext. 6573)

Abstract: In late 2013, an open call for charcoal and biochar samples was distributed in an effort to compare a wide range of char samples by Raman spectroscopy. The samples contributed to this survey included: laboratory produced biochars, recent biochars produced in field conditions, and ancient char samples previously analysed by carbon dating. By using selected Raman measurements, the char samples could be ranked in terms of the degree of thermochemical alteration or extent of carbon nanostructural development. The Raman results for recently produced biomass chars were generally consistent with the conversion of amorphous carbon formed at lower temperatures into condensed, polyaromatic, and graphene-like carbon formed at higher temperatures. A number of parameters calculated from the Raman spectra could be used to estimate the effective heat treatment temperatures in the recently produced biochars. Other samples such as anthracite coal, tire pyrolysis carbon, and ancient chars departed from the trends observed in the recently produced biomass chars using this approach. In total, 45 samples were analysed by Raman spectroscopy for this survey. Ancient and buried char samples displayed higher intensities for features in the Raman spectra associated with amorphous carbon.

Keywords: biochars; charcoal; char; Raman spectroscopy



Citation: McDonald-Wharry, J.
2013–2014 Survey of Chars Using
Raman Spectroscopy. *C* **2021**, *7*, 63.
<https://doi.org/10.3390/c7030063>

Academic Editor: Francois Normand

Received: 30 June 2021
Accepted: 8 August 2021
Published: 19 August 2021

Publisher's Note: MDPI stays neutral with regard to jurisdictional claims in published maps and institutional affiliations.



Copyright: © 2021 by the author. Licensee MDPI, Basel, Switzerland. This article is an open access article distributed under the terms and conditions of the Creative Commons Attribution (CC BY) license (<https://creativecommons.org/licenses/by/4.0/>).

1. Introduction

Chars can be produced using a wide range of different biomass precursors and using a variety of different processing technologies [1]. Even within a single processing technology, the production conditions can often be varied by altering factors such as the heat treatment temperatures and the amount of time the material spends at elevated temperatures. These precursor and processing variables mean that chars (or biochars) represent a wide range of different materials with a range of morphologies, porosities, nanostructure, chemistry, and properties. Identifying which of types of chars which are suitable for specific applications, making comparisons between different chars which feature in research literature, and quality control of manufactured chars will require methodologies for analysing and grading these carbonaceous materials. Production temperature is widely regarded to be one of the most important factors for the development of the carbon chemistry/nanostructure within the chars and the highest heat treatment temperature (HTT) is used as a common signpost for charring intensity or the degree of thermochemical alteration/transformation [2,3].

Raman spectroscopy can be used as a rapid, non-destructive technique for analysing the chemical structure of samples. Raman spectrometers have become more obtainable and portable in recent decades, with different handheld devices now available [4]. A Raman instrument which uses a visible or infra-red laser is also particularly sensitive to the nanostructure of materials which are rich in sp^2 -bonded carbon and this makes the technique a valuable tool for studying many different carbon-rich materials including graphites, coals, cokes, carbon fibers, fullerenes, soots, carbon nanotubes, amorphous carbons, and different types of graphenes [5–8]. Raman spectroscopy measurements have previously been used for evaluating the heat treatment temperature (HTT) of chars produced from Japanese cedar and proposed as a means of quality control for charcoals [9]. In more recent research, wood and cellulose-based precursors have been charred and

carbonised under laboratory conditions at a range of HTTs and these researchers have reported correlations between measurements of various features in Raman spectra of chars and the HTTs used to produce those chars [6,10]. Raman spectroscopy has been also used to analyse *terra preta* char samples from locations near Manaus, Brazil [7]. *Terra preta* char-rich soils were an inspiration for the biochar concept [11,12].

This survey was aimed at trialling a Raman analysis methodology [6] on a much wider range of chars and other carbonaceous materials in order to investigate the suitability of this approach and also identify potential problems/limitations of the current methodology. Raman spectroscopy could provide a rapid screening and quality control approach for use by both producers and purchasers of biochars. However, it will be important to determine limitations of a Raman analysis approach when used to compare and grade biochars. The survey was also an opportunity to compare a wide range of chars which were being produced or studied in the years around 2013–2014. Many of the chars featured in this survey were produced using trial, prototype, or experimental equipment. There is often scope to change processing conditions in most types of equipment and some contributors of these char samples have already changed how they are producing their chars. This survey does provide a snapshot of chars produced or studied in this time and provides a means of comparing them in terms of charring intensity (or the extent of nanostructural development within the solid carbon material).

As represented in Figure 1, chars have features at multiple scales, from the larger features retained from biological structures in the plant matter such as cells, down to carbon nanostructures. Raman spectroscopy is a non-destructive characterisation technique which is well-suited to analysing the nanostructure of carbonaceous materials [5–7]. The char nanostructural development depicted in Figure 2 is similar to the dynamic molecular structure described by Keiluweit et al. [2] and a prior review paper [13], where the amorphous char produced at lower levels of charring intensity is progressively replaced by graphene-like sheets and increased fine porosity with more intense thermal treatments. These stacks of graphene-like sheets/domains in well-carbonised are often called crystals or turbostratic crystallites. However, in most chars, these stacks lack truly crystalline structure [14]. For evaluation and comparison between chars in the literature, a number of parameters are used to indicate charring intensity, degree of thermochemical alteration, or nanostructural development. These parameters include: HTT, H/C_{org} ratios, fixed carbon content, and degree of aromatic condensation [2,3,15,16]. With the development of carbon nanostructure (or increase in charring intensity), a range of properties of chars change greatly. These changes include increases in hardness [17], fine porosity/surface area [2], electrical conductivity [10,18] and stability [15,19]. With the intensity of heat treatment (and the resulting carbon nanostructure) being the major determinant of biochar properties, the capability to rapidly assess char nanostructure provided by Raman spectrometry has value in assessing biochar quality. As demonstrated in Figure 2, the number of features in the Raman spectra recorded from char samples change based on the type of carbon chemistry/nanostructures found within the various chars. Measuring the intensity of various features in the Raman spectrum (such as height of the valley or D band) relative to another features (usually the height of the G band as it is often the most intense feature) provides a number of ratio values that can be used to assess and compare char samples.

As the carbon nanostructure develops (typically as the HTT used to produce the char or charring intensity is increased), the following changes have been found to occur in the Raman spectra [6]:

- Decreases in the Valley/G band height ratio (interpreted as the removal of amorphous carbon).
- Decreases in the A band/G band height ratio (interpreted as the removal of amorphous carbon).
- Decreases in the slope/G band height ratio (interpreted as the removal of hydrogen-rich amorphous carbon which causes this intense photoluminescence slope).

- Increases in the D band/G band height ratio (interpreted as the lateral extension of graphene-like polyaromatic domains as they organise and grow towards being a few nanometres across).
- Increases in the apparent position of the G band from around 1500 cm^{-1} to 1600 cm^{-1} (interpreted as organising of the carbon into larger clusters/domains of aromatic carbon, changes in level of strain on carbon-carbon bonds, and/or the effect of overlapping bands).

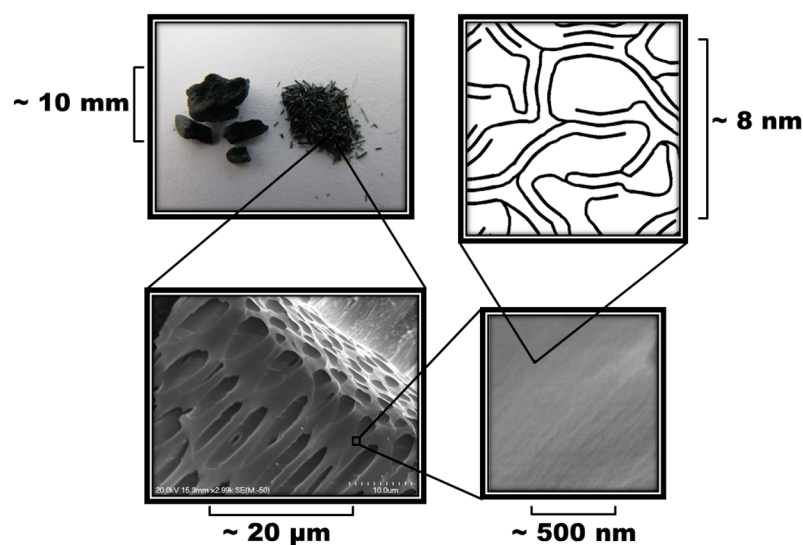


Figure 1. Features of biomass chars at various length scales [20]. Top left are structures which can be seen with the eye and easily photographed. The bottom two images are microscopic features which can be observed with scanning electron microscopes. The top-right sketch represents the nanostructure of well-carbonised chars where most of the carbon is part of interconnected graphene-like layers forming disordered stacks and nanometre-scale porosity.

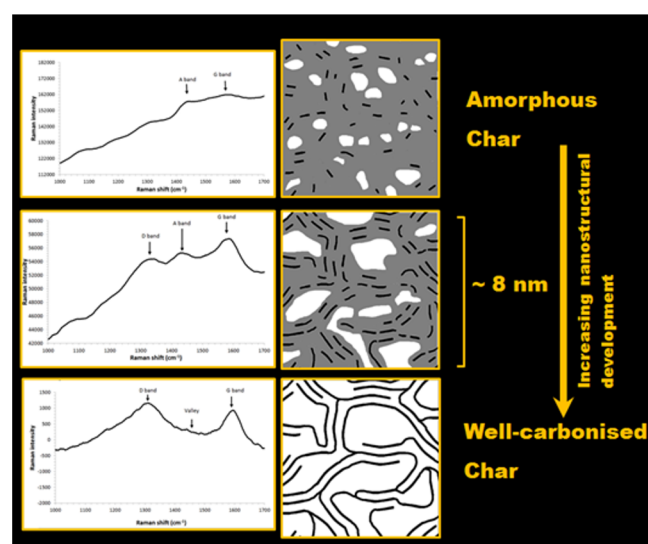


Figure 2. Sketches providing an overview of how features in Raman spectra of chars change as the extent of nanostructural development (or charring intensity) increases. In the illustrations of the char nanostructure, the black lines represent clusters of aromatic carbon which grow into a tangle of cross-linked graphene-like domains and the grey colour represents regions of hydrogen-rich amorphous carbon.

2. Materials and Methods

Following a call for biochars and other char samples in late 2013, a range of individuals and groups contributed samples of biochars and other carbonaceous materials to this survey. For these samples, details about their production or origin along with references for samples featured in other publications are provided in Table 1. Three of the samples originated from Europe and were samples of the chars from the COST interlaboratory comparison [21]. Most of the survey samples were sent in from around the Pacific Ocean including New Zealand, Malaysia, Yap, Australia, Hawaii, and Oregon. Some examples of non-biochar carbonaceous materials were also included. These samples include a carbonaceous residue from tire pyrolysis carbon and an anthracite coal standard. A sample of ancient oak charcoal from an Irish archaeological site (dated to around 3700 years old) was included along with two samples of thermally modified wood recovered from volcanic ash deposits from Rotomahana tephra/mud in New Zealand (~129 years old, [22]) and Noname beach tephra in Australia (~92,000 years old [23]).

Raman spectra were acquired using a Ramanstation™ 400 instrument (PerkinElmer) equipped with a 785 nm laser. Each sample was mixed and five randomly selected surfaces (sub-samples) of the as-received samples were analysed. Each sub-sample Raman spectrum was collected from a spot (100–300 µm in diameter) using five consecutive exposures to the laser. Twenty second exposure times were used routinely with an alternative of five second exposure times occasionally used on lower HTT chars to avoid detector saturation. The instrument settings, data processing procedure and interpretation of spectral features are detailed in previously published research [6]. Note that many Raman signals from carbonaceous materials are dispersive, meaning that their positions and intensities can change based on the excitation wavelength used by the instrument [24,25]. Therefore, caution should be used when comparing Raman results from different laser-types and different instruments.

Table 1. Sample details provided by contributors and references were chars feature in other publications.

Sample Short Name	Precursor and Preparation Details	Contributors and References to Other Research Involving These Samples
BSe-250 BSe-350 BSe-450 BSe-550 MAe-250 MAe-350 MAe-450 BSe-250 HF BSe-350 HF BSe-450 HF BSe-550 HF MAe-250 HF MAe-350 HF MAe-450 HF	Precursor: Biosolids and eucalyptus (1:1 by dry weight) Production: Slow pyrolysis in lab scale gas-fired drum Notes: Number indicates target processing temperature in °C Precursor: Cattle manure and eucalyptus (1:1 by dry weight) Production: Slow pyrolysis in lab scale gas-fired drum Notes: Number indicates target processing temperature in °C Same as the above samples, except these sub-samples labelled HF had been treated after pyrolysis with 10% Hydrofluoric acid 4 times each to remove approximately 70% of the ash content	Tao Wang, New Zealand Biochar Research Centre, Massey University [16,26]
Massey open source (Run 5)	Precursor: <i>Pinus Radiata</i> woodchips Production: Open-source batch pyrolyser, HTT ≈ 705 °C	Rhonda Bridges, Jim Jones, Massey University [27]
UC slow Pyrolysis UC fast Pyrolysis	Precursor: <i>Pinus Radiata</i> sawdust Production: Slow pyrolysis Precursor: <i>Pinus Radiata</i> sawdust Production: Fast pyrolysis	Tansy Wigley, Shusheng Pang, Alex Yip, University of Canterbury

Table 1. Cont.

Sample Short Name	Precursor and Preparation Details	Contributors and References to Other Research Involving These Samples
Anthracite coal Rotomahana tephra Noname beach (Australian tephra) Ancient oak	Gronigen coal Char recovered from tephra, water washed Wood recovered from approximately 92-thousand-year-old tephra, HCl washed Oak from N11 Rathnew–Arklow Archaeological site in Ireland dated to around 3700 years old	Fiona Petchey, University of Waikato Radiocarbon Dating Laboratory The ‘Noname beach’ sample has featured in this recent study [23]
Leucan metal kiln	Precursor: <i>Leucan Insularum</i> wood Production: Metal kiln	Frank Cushing and Marjorie Falanrum, Yap Institute of Natural Sciences
Fluidyne gasifier	Precursor: <i>Pinus Radiata</i> wood Production: Fluidyne Down Draught Pioneer engine gasifier. Process temperatures: 1200–1500 °C	Doug Williams
Domestic log fire (water quenched) Domestic log fire (air cooled)	Precursor: Acacia wood Production: Log placed in domestic fire for 20 min and removed as red/orange embers which were either quenched in cold water or left to cool in air	John McDonald-Wharry
Yealand’s Estate Batch Yealand’s Estate Auger	Precursor: Grape prunings Production: Batch Precursor: Grape prunings Production: Auger	Aaron Black, Yealand’s Estate
Giant reed Tasmanian blackwood	Precursor: Giant Reed (<i>Arundo Donax</i>) Production: Batch, double-drum retort Precursor: Tasmanian blackwood (<i>Acacia Melanoxylon</i>) Production: Batch, double-drum retort	Jim Hunt
Cone kiln (TFOD)	Precursor: Douglas fir mill ends Production: Cone kiln, top-fed open draft device (TFOD)	Kelpie Wilson
Tyre pyrolysis carbon	Precursor: End-of-life tires Production: Destructive distillation	Trevor Bayley, Green Distillation Technologies Corporation Ltd.
Flash oak bottom Flash oak middle Flash corn bottom	Precursor: Cowboy oak wood sawdust Production: Flash carbonization Precursor: Cowboy oak wood sawdust Production: Flash carbonization Precursor: Waimanalo corn cob Production: Flash carbonization	Michael J Antal Jr. Hawaii Natural Energy Institute, University of Hawaii at Manoa [28,29]
Rice husk char	Precursor: Rick husk Production: Double cyclone furnace (direct heating/combustion system; 2000 kW/hr; rice husk fuel for rice drying in rice mill)	Trevor Richards, Biochar Systems Limited. Kilang Beras Saudara Ban Eng Hin SDn. Bhd.
Coconut shell char Mixed sawdust Kiln Palm empty fruit bunch	Precursor: Coconut shell Production: Typical raw product for the activated carbon market. Precursor: Mixed forest sawdust Production: Typical ‘Japanese-type’ kilns operated at 700–800 °C Precursor: Empty fruit bunch from oil palm Production: Nasmach	Trevor Richards, Biochar Systems Limited. Various sources
COST I COST II COST III	Precursor: Mixed wood shavings Production: Pyreg 500-III pyrolysis unit (620 °C) Precursor: Paper sludge and wheat husks Production: Pyreg 500-III pyrolysis unit (500 °C) Precursor: Sewage sludge Production: Pyreg 500-III pyrolysis unit (600 °C)	EU-COST Action on Biochar WG1, [21,30]

Table 1. Cont.

Sample Short Name	Precursor and Preparation Details	Contributors and References to Other Research Involving These Samples
TLUD top middle	Precursor: Pine woodchips Production: Top-lit updraft gasifier (TLUD) Sample taken from middle of the top of the char bed.	Earl Mardle
Stardust Continuous	Precursor: Pine woodchips Production: Continuous auger pyrolyser	Simon Day

3. Results

Based on correlations found between the HTTs and Raman results in a previous study of low-ash chars [6], ‘effective HTT values’ could be calculated for each sample in the survey. These Raman-estimated ‘effective HTT values’ are based on comparisons to laboratory chars which were raised to the highest temperature and held at that temperature for 10–20 min. This Raman method focused on detecting the nanostructural development, which typically occurs between 350 °C and 700 °C. Using the apparent position of the G band or the ratio between the valley height (located between the D band and G band) and the G band height, the ‘effective HTT values’ for char samples within this range could be estimated (Figure 3). The char samples are ranked according to G band position along the X-axis of graphs in Figures 3–5. This approximately orders the chars from well-carbonised on the left side through to the least carbonised on the right side.

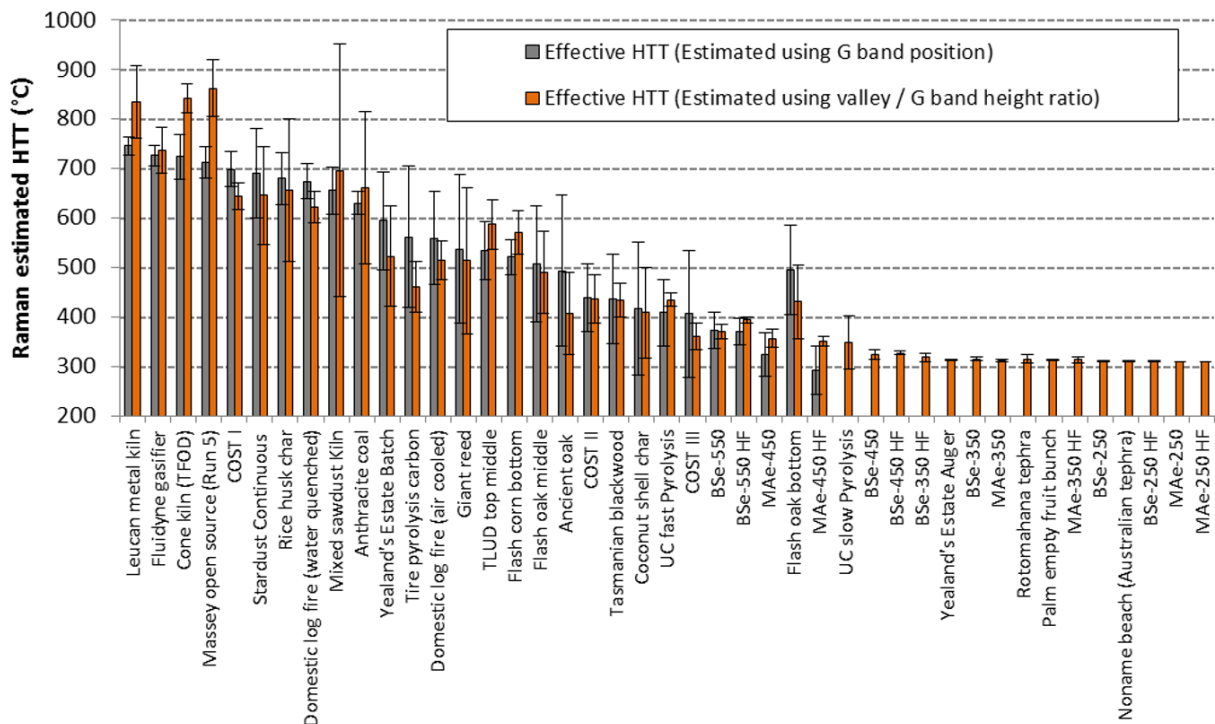


Figure 3. Raman estimated effective HTTs. Samples are ranked along X-axis from highest value of apparent G band position on the left to lowest on the right. Error bars represent 99% confidence intervals.

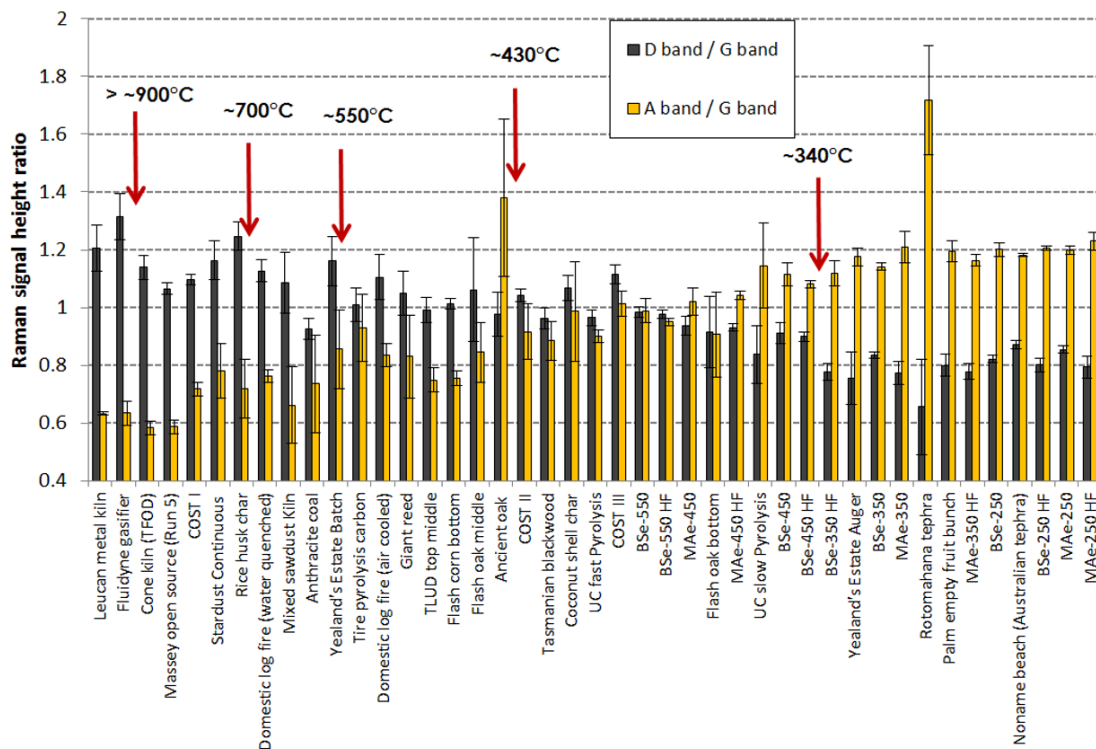


Figure 4. Measured heights of the D band and A band relative to the G band. Samples are ranked along X-axis from highest value of apparent G band position on the left to lowest on the right. Error bars represent 99% confidence intervals. Red arrows indicate where chars prepared at a range of heat treatment temperatures (HTTs) in laboratory furnaces (with ~20 min dwell once at peak temperature) and analysed previously would be placed according to this G band position ranking system.

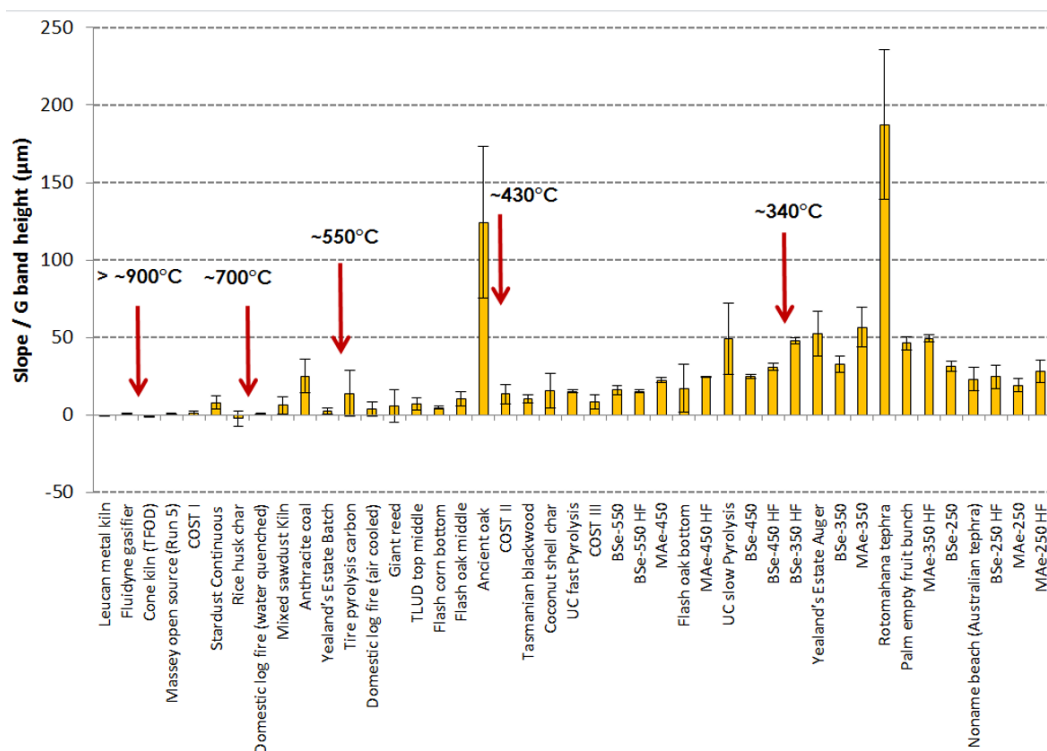


Figure 5. Slope value relative to the G band height. Samples are ranked along X-axis from the highest value of apparent G band position on the left to lowest on the right. Error bars represent 99% confidence intervals. Large positive values for this slope-based parameter indicate hydrogen-rich amorphous carbon. These red arrows are used for approximate signposts for “effective HTT” based on comparisons to a set of laboratory produced chars.

The current Raman method is not optimised to analyse the extremely amorphous (and/or non-charred) samples produced at very low HTT, and as indicated by the lack of Raman, estimated HTT values based on G band position for those samples in Figure 3. The results indicate that the correlation between G band position and effective HTT changes near an effective HTT of 360 °C. A new calibration between Raman measurements with char HTTs below 360 °C could be possible; however, laboratory chars prepared below 360 °C tend to be highly variable and it is difficult to produce standard chars at these low heat treatment temperatures. Towards the right side of Figures 3–5 sit the brown non-charred (torrefied) samples such as the BSe-250, MAe-250, and the Noname Beach sample of wood (which is assumed to have been mildly thermally altered by hot volcanic ash). In Figures 4 and 5, red arrows indicate where previously analysed chars prepared at a range of HTTs in laboratory furnaces would be placed according to the ranking system based on G band position. These red arrows are used as approximate signposts for “effective HTT” based on comparisons to a set of laboratory produced chars [6,31]. Tabulated results from the analysis of the Raman spectra can be found in Supplementary Materials, Table S1.

4. Discussion

4.1. Raman Analysis

When comparing and analysing Raman spectra of carbonaceous material, be aware that peaks (especially the D band and what is labelled the A band) can shift position and intensity depending on the wavelength of laser used by the Raman instruments [24]. Across the scientific literature, there are also a number of different ways of assigning peaks or measuring values. Some researchers measure peak areas, others use peak heights, and there are different approaches for subtracting sloping backgrounds and the deconvolution of overlapping signals [32] and this means that using a consistent data processing method is important for comparing samples. Note that in the current approach, the apparent heights and positions of Raman features such as the G band are analysed without deconvolution. Although this provides a simple approach to rapidly compare char samples, it is acknowledged that in some cases, a parameter such as ‘apparent G band position’ will have a contribution from other overlapping signals such as the D’ band which occurs near 1620 cm⁻¹ [5]. Another potential problem with Raman analysis is that excessive or concentrated laser power could burn or further carbonise the surface of the sample. This Raman method uses reduced laser power (20% of maximum) and analyses a relatively large spot (100–300 µm), which reduces the risk of excessive sample heating.

4.2. Recently-Produced Biochar Samples

As can be observed in Figure 4, the recently produced biochars followed a pattern of increasing D band/G band height ratios and decreasing A band/G band height ratios when ranked according to increasing G band position values. Along with the valley/G band height ratio (Figure 3), these approaches can be used to compare recently produced chars in terms of the ‘extent of nanostructural development’. Certain field-produced biochar samples, such as the ‘Leucan metal kiln’ and ‘Cone kiln, top-fed open draft device (TFOD)’, were found to have the highest extent of nanostructural development of the chars in this survey, higher than the laboratory-produced chars. The top 5 char samples at the well-carbonised side of the results charts (left-hand side of Figures 3 and 4) were a mixture of batch and continuous chars, indicating that similar quality carbon nanostructures can readily be produced using either type of process. Towards the least-carbonised end (right-hand side) of the results charts, these char samples are more suited to assessment using parameters related to hydrogen-rich amorphous carbon content such as the A band/G band height ratio (Figure 4) and the background slope value relative to the G band height (Figure 5).

4.3. Non-Biochar Samples

The carbonaceous samples that were not recently produced biomass chars (such as the anthracite coal, tire pyrolysis carbon, and two char samples from archaeological/volcanic sites) appeared as significant deviations from the overall trends for chars in Figure 4. The anthracite coal sample had a lower D band/G band height ratio than neighbouring chars given its G band position-based rank (Figure 4). This indicates smaller graphene-like domains in the coal sample and/or potentially greater compressive stress on the domains with this likely relating to differences in coal formation (presumably formed at lower temperatures and under compressive stress [33]). There was considerable variation in sub-sample spectra of anthracite coal, with some spectra having amorphous features similar to those found in very low HTT chars and other spectra having features similar to those of well-carbonised chars with apparent overlap in most coal sub-samples. Certain components (macerals) of coals, known as fusinite [34] or fusian [35,36], are considered to have a pyrogenic origin as chars. They are formed in higher temperature vegetation fires then deposited into the organic material, which is eventually formed into coal (Fusian can make up 10–20% of some coals [36]). The tire pyrolysis carbon sub-samples also demonstrated considerable variability with regions of reasonably well-carbonised material (presumably from the carbon black component of the tires) and a more amorphous material (presumably formed in the pyrolysis process reported to operate around 410 °C) which appeared to overlap in many sub-samples.

The sample labelled ancient oak was a char sample recovered from an archaeological site in Ireland (carbon dated to around 3700 years old). Both this oak char sample and a char sample recovered from a volcanic ash layer (Rotomahana tephra, approximately 129 years old) featured A band signals of extremely high relative intensity (Figure 4) and large values for the photoluminescence slope/G band height (Figure 5). Measurements of this positive slope in the Raman spectra have previously been proposed as a way of quantifying the contamination of archaeological charcoal samples with humic substances [37]. However, some humic substances (“pyromorphic humus”) are considered to be formed during pyrolysis or due to char alteration, degradation and oxidation [38–40]. Therefore, these high values of Raman signals, which are interpreted as additional amorphous carbon (slope and A band in the Raman spectra), might instead relate to aging (oxidation) of these chars. Previous Raman analysis of *terra preta* grains reported that the surfaces were more amorphous/disordered than the core of the grains and this was interpreted as indicating oxidation of the surfaces [7], with a prominent positive sloping baseline also being a feature of the *terra preta* samples. A recent paper comparing aged and fresh chars demonstrated higher photoluminescence slope/G band height values for the aged chars extracted from soils in Japan [41].

4.4. High-Ash Biochars

The chars with very high inorganic contents (in case of the COST III sample, ~74% ash by weight [21]) that were produced using large proportions of manures and sewage biosolids as feedstocks were found by this Raman analysis to be less nanostructurally developed than expected given the production temperatures reportedly used in their manufacture. This could potentially be inorganic materials interfering with the Raman analysis; however, the hydrofluoric acid-extracted samples of the BSe and MAe chars produced similar spectra to the non-extracted samples, indicating that these inorganic materials only cause minor contributions/interference to these Raman spectra. Higher H/C ratios were reported for these samples in previous chemical analysis [16,26]. This supports the conclusion that these chars produced using manure/biosolid precursors have a less developed carbon nanostructure/chemistry when compared to chars produced from low-ash precursors when both are produced under similar production temperatures. Similar results have been found in other studies with manure-derived chars featuring less developed carbon structures (more non-aromatic carbon and small domains of condensed

aromatic carbon) when compared to low-ash, wood-derived chars or leaf-derived chars prepared under the same conditions [15].

The high ash content in some chars can interfere with measurements of the slope value because some inorganic materials generate a negative fluorescence contribution to the slopes [4]. This is the likely cause of some negative slope values obtained for the rice husk and giant reed chars in Figure 5, and will mean that additional caution is needed when interpreting slope-based measurements in ash-rich chars. Two char samples made from biosolids and wood chips (BSe-350 and BSe-450) had significantly higher photoluminescence slope/G band height values after hydrofluoric acid extraction (Figure 5). This indicates that the inorganic content present made a negative contribution to the overall background slope and the removal of these inorganic materials leads to larger positive slope values.

4.5. Potential Future Research

A wider selection of coals and humic materials could be analysed with this method for comparison with the chars. More examples of aged/weathered chars which have been in soil should be analysed to determine if the unusual results obtained for the few old chars included in this survey are common to aged chars generally. Further investigation of the structural/chemical changes that might occur over time in chars is warranted and the potential relationship between humic materials and chars needs to be studied in more depth (such as potential adsorption of humic substances on to the chars or transformation of a portion of the char into humic substances with aging).

Raman results need to be correlated to other measurements and properties of chars. Properties which are directly related to carbon nanostructure such as electrical conductivity, hardness and surface area associated with nanometre-sized porosity should correlate with Raman parameters (although ash content might interfere with some of these correlations). The valley/G band height ratio is hypothesised to correlate with volatile matter/fixed carbon ratios. Some initial correlations have been found between Raman measurements of nanostructural development and the H/C ratios for pine chars produced at a range of HTTs between 340 °C and 700 °C [42]. It needs to be established if these correlations hold true when chars prepared from other precursors are analysed. Nuclear magnetic resonance (NMR) measurements of non-aromatic carbon and degree of aromatic condensation have previously been used to estimate the stability of biochars [15]. Given that Raman spectroscopy is also providing information about these types of changes in carbon structure, there is scope to correlate Raman measurements to similar stability estimates in the future. If a similar Raman survey is able to be conducted in the future, it will be interesting to see if a change in distribution of chars occurs as research and production becomes focused on specific types of chars optimised for specific applications.

5. Conclusions

A wide range of chars and other carbonaceous materials were provided for this Raman survey and these samples represented a diverse selection of precursors and different production methods. Raman-based measurements were used to rank chars according to charring intensity or extent of nanostructural development within the carbon constituents. The Raman results obtained from the recently produced chars in this survey were consistent with expected trends and ranged from high-temperature well-carbonised chars which had Raman spectra featuring signals of disordered graphene-like structures through to amorphous chars prepared at lower temperatures. High-ash manure/biosolids-derived chars appeared to have less developed carbon nanostructures for the temperatures used in their production when compared to chars produced from low-ash precursors such as wood. Some wood biochars produced with field production technologies (such as kilns) produced well-carbonised chars with the Raman analysis indicating levels of nanostructural development similar to char produced in laboratory conditions with heat-treatment temperatures above 700 °C. By comparing multiple Raman measurements, non-biochar

carbonaceous samples such as tire-pyrolysis carbon and anthracite coal could be identified as not following the overall trends in found in the recently produced char samples.

Supplementary Materials: The following are available online at <https://www.mdpi.com/article/10.3390/c7030063/s1>, Table S1: 2013–2014 Survey of Chars Using Raman Spectroscopy.

Funding: This research received no external funding.

Data Availability Statement: Please contact the author if Raman analysis datasets are required.

Acknowledgments: The author would like to thank all the contributors which provided samples for this survey: Tao Wang, Tansy Wigley, Shusheng Pang, Alex Yip, Kelpie Wilson, Fiona Petchey, Roberto Calvelo Pereira, Hans-Peter Schmidt, Frank Cushing, Marjorie Falanrum, Doug Williams, Aaron Black, Jim Hunt, Trevor Bayley, Michael J Antal Jr., Trevor Richards, Earl Mardle, Simon Day, Jim Jones, Georg Ripberger, and Rhonda Bridges. John McDonald-Wharry was supported by The University of Waikato Doctoral Scholarship and acknowledges the advice provided by Merilyn Manley-Harris and Kim Pickering during that PhD project.

Conflicts of Interest: The author declares no conflict of interest.

References

- Meyer, S.; Glaser, B.; Quicker, P. Technical, economical, and climate-related aspects of biochar production technologies: A literature review. *Environ. Sci. Technol.* **2011**, *45*, 9473–9483. [[CrossRef](#)] [[PubMed](#)]
- Keiluweit, M.; Nico, P.S.; Johnson, M.G.; Kleber, M. Dynamic molecular structure of plant biomass-derived black carbon (biochar). *Environ. Sci. Technol.* **2010**, *44*, 1247–1253. [[CrossRef](#)]
- Antal, M.J.; Grønli, M. The art, science, and technology of charcoal production. *Ind. Eng. Chem. Res.* **2003**, *42*, 1619–1640. [[CrossRef](#)]
- Jehlička, J.; Culka, A.; Bersani, D.; Vandenebeele, P. Comparison of seven portable Raman spectrometers: Beryl as a case study. *J. Raman Spectrosc.* **2017**, *48*, 1289–1299. [[CrossRef](#)]
- Cuesta, A.; Dhamelincourt, P.; Laureyns, J.; Martinezalonso, A.; Tascon, J.M.D. Raman microprobe studies on carbon materials. *Carbon* **1994**, *32*, 1523–1532. [[CrossRef](#)]
- McDonald-Wharry, J.; Manley-Harris, M.; Pickering, K. Carbonisation of biomass-derived chars and the thermal reduction of a graphene oxide sample studied using Raman spectroscopy. *Carbon* **2013**, *59*, 383–405. [[CrossRef](#)]
- Ribeiro-Soares, J.; Cançado, L.G.; Falcão, N.P.S.; Martins Ferreira, E.H.; Achete, C.A.; Jorio, A. The use of Raman spectroscopy to characterize the carbon materials found in Amazonian anthrosoils. *J. Raman Spectrosc.* **2012**, *44*, 283–289. [[CrossRef](#)]
- Sadezky, A.; Muckenhuber, H.; Grothe, H.; Niessner, R.; Pöschl, U. Raman microspectroscopy of soot and related carbonaceous materials: Spectral analysis and structural information. *Carbon* **2005**, *43*, 1731–1742. [[CrossRef](#)]
- Yamauchi, S.; Kurimoto, Y. Raman spectroscopic study on pyrolyzed wood and bark of Japanese cedar: Temperature dependence of Raman parameters. *J. Wood Sci.* **2003**, *49*, 235–240. [[CrossRef](#)]
- Rhim, Y.R.; Zhang, D.J.; Fairbrother, D.H.; Wepasnick, K.A.; Livi, K.J.; Bodnar, R.J.; Nagle, D.C. Changes in electrical and microstructural properties of microcrystalline cellulose as function of carbonization temperature. *Carbon* **2010**, *48*, 1012–1024. [[CrossRef](#)]
- Glaser, B.; Birk, J.J. State of the scientific knowledge on properties and genesis of Anthropogenic Dark Earths in Central Amazonia (terra preta de Índio). *Geochim. Cosmochim. Acta* **2012**, *82*, 39–51. [[CrossRef](#)]
- Lehmann, J.; Gaunt, J.; Rondon, M. Bio-char sequestration in terrestrial ecosystems—A review. *Mitig. Adapt. Strateg. Glob. Chang.* **2006**, *11*, 395–419. [[CrossRef](#)]
- McDonald-Wharry, J.; Manley-Harris, M.; Pickering, K. Understanding and visualising the nanostructural development of chars during carbonisation. In Proceedings of the 3rd Asia Pacific Biochar Conference, Chuncheon, Korea, 19–23 October 2016.
- Franklin, R.E. Crystallite growth in graphitizing and non-graphitizing carbons. *Proc. R. Soc. Lond. Ser. A Math. Phys. Sci.* **1951**, *209*, 196–218.
- Singh, B.P.; Cowie, A.L.; Smernik, R.J. Biochar carbon stability in a clayey soil as a function of feedstock and pyrolysis temperature. *Environ. Sci. Technol.* **2012**, *46*, 11770–11778. [[CrossRef](#)]
- Wang, T.; Camps-Arbestain, M.; Hedley, M. Predicting C aromaticity of biochars based on their elemental composition. *Org. Geochem.* **2013**, *62*, 1–6. [[CrossRef](#)]
- Zickler, G.A.; Schoberl, T.; Paris, O. Mechanical properties of pyrolysed wood: A nanoindentation study. *Philos. Mag.* **2006**, *86*, 1373–1386. [[CrossRef](#)]
- Mochidzuki, K.; Soutric, F.; Tadokoro, K.; Antal, M.J., Jr.; Toth, M.; Zelei, B.; Varhegyi, G. Electrical and physical properties of carbonized charcoals. *Ind. Eng. Chem. Res.* **2003**, *42*, 5140–5151. [[CrossRef](#)]
- Crombie, K.; Mašek, O.; Sohi, S.P.; Brownsort, P.; Cross, A. The effect of pyrolysis conditions on biochar stability as determined by three methods. *GCB Bioenergy* **2013**, *5*, 122–131. [[CrossRef](#)]

20. McDonald-Wharry, J.S.; Manley-Harris, M.; Pickering, K.L. Reviewing, combining, and updating the models for the nanostructure of non-graphitizing carbons produced from oxygen-containing precursors. *Energy Fuels* **2016**, *30*, 7811–7826. [[CrossRef](#)]
21. Bachmann, H.J.; Bucheli, T.D.; Dieguez-Alonso, A.; Fabbri, D.; Knicker, H.; Schmidt, H.-P.; Ulbricht, A.; Becker, R.; Buscaroli, A.; Buerge, D.; et al. Toward the standardization of biochar analysis: The COST action TD1107 interlaboratory comparison. *J. Agric. Food Chem.* **2016**, *64*, 513–527. [[CrossRef](#)]
22. Berryman, K.; Villamor, P.; Nairn, I.; van Dissen, R.; Begg, J.; Lee, J. Late Pleistocene surface rupture history of the Paeroa Fault, Taupo Rift, New Zealand. *N. Z. J. Geol. Geophys.* **2008**, *51*, 135–158. [[CrossRef](#)]
23. Ascough, P.L.; Brock, F.; Collinson, M.E.; Painter, J.D.; Lane, D.W.; Bird, M.I. Chemical characteristics of macroscopic pyrogenic carbon following millennial-scale environmental exposure. *Front. Environ. Sci.* **2020**, *7*, 203. [[CrossRef](#)]
24. Ferrari, A.C.; Robertson, J. Interpretation of Raman spectra of disordered and amorphous carbon. *Phys. Rev. B* **2000**, *61*, 14095–14107. [[CrossRef](#)]
25. Veres, M.; Tóth, S.; Koós, M. New aspects of Raman scattering in carbon-based amorphous materials. *Diam. Relat. Mat.* **2008**, *17*, 1692–1696. [[CrossRef](#)]
26. Wang, T. Development of Methodologies for the Characterisation of Biochars Produced from Human and Animal Waste. Ph.D. Thesis, Massey University, Palmerston North, New Zealand, 2013.
27. Bridges, R. Design and Characterisation of an “Open Source” Pyrolyser for Biochar Production. Master’s Thesis, Massey University, Palmerston North, New Zealand, 2013.
28. Wang, L.; Skreiberg, Ø.; Gronli, M.; Specht, G.P.; Antal, M.J. Is elevated pressure required to achieve a high fixed-carbon yield of charcoal from biomass? Part 2: The importance of particle size. *Energy Fuels* **2013**, *27*, 2146–2156. [[CrossRef](#)]
29. Wang, L.; Trninic, M.; Skreiberg, Ø.; Gronli, M.; Considine, R.; Antal, M.J. Is elevated pressure required to achieve a high fixed-carbon yield of charcoal from biomass? Part 1: Round-robin results for three different corncob materials. *Energy Fuels* **2011**, *25*, 3251–3265. [[CrossRef](#)]
30. Schmidt, H.-P.; Bachmann, H.J.; Bucheli, T.; Fabbri, D.; Knicker, H.; Ulbricht, A. Analytical Standards for Biochar Characterization and Certification: Lessons from the EU-COST Ring Trial. 2014.
31. McDonald-Wharry, J.; Manley-Harris, M.; Pickering, K. A comparison of the charring and carbonisation of oxygen-rich precursors with the thermal reduction of graphene oxide. *Philos. Mag.* **2015**, *95*, 4054–4077. [[CrossRef](#)]
32. Zickler, G.A.; Smarsly, B.; Gierlinger, N.; Peterlik, H.; Paris, O. A reconsideration of the relationship between the crystallite size L_a of carbons determined by X-ray diffraction and Raman spectroscopy. *Carbon* **2006**, *44*, 3239–3246. [[CrossRef](#)]
33. Beyssac, O.; Brunet, F.; Petit, J.-P.; Goffé, B.; Rouzaud, J.-N.I. Experimental study of the microtextural and structural transformations of carbonaceous materials under pressure and temperature. *Eur. J. Min.* **2004**, *15*, 937–951. [[CrossRef](#)]
34. Scott, A.C.; Damblon, F. Charcoal: Taphonomy and significance in geology, botany and archaeology. *Paleogeogr. Paleoclimatol. Paleoecol.* **2010**, *291*, 1–10. [[CrossRef](#)]
35. Sander, P.M.; Gee, C.T. Fossil charcoal: Techniques and applications. *Rev. Palaeobot. Palynol.* **1990**, *63*, 269–279. [[CrossRef](#)]
36. Knicker, H. Pyrogenic organic matter in soil: Its origin and occurrence, its chemistry and survival in soil environments. *Quat. Int.* **2011**, *243*, 251–263. [[CrossRef](#)]
37. Alon, D.; Mintz, G.; Cohen, I.; Weiner, S.; Boaretto, E. The use of Raman spectroscopy to monitor the removal of humic substances from charcoal; quality control for ^{14}C dating of charcoal. *Radiocarbon* **2002**, *44*, 1–11. [[CrossRef](#)]
38. Ascough, P.L.; Bird, M.I.; Francis, S.M.; Thornton, B.; Midwood, A.J.; Scott, A.C.; Apperley, D. Variability in oxidative degradation of charcoal: Influence of production conditions and environmental exposure. *Geochim. Cosmochim. Acta* **2011**, *75*, 2361–2378. [[CrossRef](#)]
39. Mao, J.D.; Johnson, R.L.; Lehmann, J.; Olk, D.C.; Neves, E.G.; Thompson, M.L.; Schmidt-Rohr, K. Abundant and Stable Char Residues in Soils: Implications for Soil Fertility and Carbon Sequestration. *Environ. Sci. Technol.* **2012**, *46*, 9571–9576. [[CrossRef](#)] [[PubMed](#)]
40. Haumaier, L.; Zech, W. Black carbon—Possible source of highly aromatic components of soil humic acids. *Org. Geochem.* **1995**, *23*, 191–196. [[CrossRef](#)]
41. Inoue, J.; Yoshie, A.; Tanaka, T.; Onji, T.; Inoue, Y. Disappearance and alteration process of charcoal fragments in cumulative soils studied using Raman spectroscopy. *Geoderma* **2017**, *285*, 164–172. [[CrossRef](#)]
42. McDonald-Wharry, J.; Ripberger, G.; Manley-Harris, M.; Pickering, K. Studying carbonisation with Raman spectroscopy. In Proceedings of the New Zealand Biochar Workshop, Palmerston North, New Zealand, 4–5 July 2013.